Rethinking End-to-End 2D to 3D Scene Segmentation in Gaussian Splatting

Runsong Zhu[1] Shi Qiu[1] Zhengzhe Liu[2,3] Ka-Hei Hui[1] Qianyi Wu[4]
Pheng-Ann Heng[1] Chi-Wing Fu[1]
[1]The Chinese University of Hong Kong [2] Lingnan University
[3] Carnegie Mellon University [4] Monash University

Abstract

Lifting multi-view 2D instance segmentation to a radiance field has proven to be effective to enhance 3D understanding. Existing methods rely on direct matching for end-to-end lifting, yielding inferior results; or employ a two-stage solution constrained by complex pre- or post-processing. In this work, we design a new end-to-end object-aware lifting approach, named Unified-Lift that provides accurate 3D segmentation based on the 3D Gaussian representation. To start, we augment each Gaussian point with an additional Gaussian-level feature learned using a contrastive loss to encode instance information. Importantly, we introduce a learnable object-level codebook to account for individual objects in the scene for an explicit object-level understanding and associate the encoded object-level features with the Gaussian-level point features for segmentation predictions. While promising, achieving effective codebook learning is non-trivial and a naive solution leads to degraded performance. Therefore, we formulate the association learning module and the noisy label filtering module for effective and robust codebook learning. We conduct experiments on three benchmarks: LERF-Masked, Replica, and Messy Rooms datasets. Both qualitative and quantitative results manifest that our Unified-Lift clearly outperforms existing methods in terms of segmentation quality and time efficiency.

1. Introduction

Accurate 3D scene segmentation enhances scene understanding and facilitates scene editing, benefiting many downstream applications in virtual reality, augmented reality, and robotics. However, accurate 3D scene segmentation is challenging to obtain, due to limited 3D dataset size and labor-intensive manual labeling in 3D. To bypass these challenges, recent studies [1, 33, 44] suggest lifting 2D segmentations predicted by foundation models [3, 15] to the 3D scene modeled by a radiance field for instance-level understanding. Yet, 2D instance segmentations predicted by models like SAM [15] lack consistency across different views, *e.g.*, the same object may have different IDs when viewed from different angles, leading to conflicting supervision. Besides, inferior segmentations, *e.g.*, under- or over-segmentation, make the lifting process challenging.

Various strategies have been proposed to address the above issues. An early work Panoptic Lifting [33] trains a NeRF to render instance predictions in an end-to-end manner and matches the model's 3D predictions with the initial 2D segmentation masks to provide supervision. However, this approach tends to produce multi-view inconsistent segmentation as it is highly sensitive to the variances of matching results. Subsequently, [23, 39] propose object association techniques as a preprocessing to prepare view-consistent 2D segmentation maps with improved multi-view consistency (see Fig. 1 (b)). However, the preprocessing stage often struggles to produce accurate results and the accumulated error can further degrade the performance. The recent state-of-the-art methods [1, 40] encode instance information in the feature field using contrastive learning and apply a clustering as a postprocessing to produce the final segmentations (see Fig. 1 (c)). Though significant improvements are achieved, their performance is always constrained by the naive clustering postprocess, which is hyperparameter-sensitive and also induces error accumulation. Given the above concerns, we come up with this question: *"Can we have an end-to-end lifting framework for accurate 3D scene segmentation, without the need of pre- or post-processing?"*

In this work, we propose a new end-to-end object-aware lifting method called Unified-Lift for accurate 3D scene segmentation, facilitating the generation of coherent and view-consistent instance segmentation across different views. We exploit the recent advancement of the radiance field, *i.e.*, 3D Gaussian splatting (3D-GS) [12], as the 3D scene representation due to its superior efficiency and rendering quality. Specifically, we augment each Gaussian point in 3D-GS with a Gaussian-level feature and learn these features using contrastive learning defined in each individual view. In particular, we introduce a novel global object-level codebook to represent each ob-

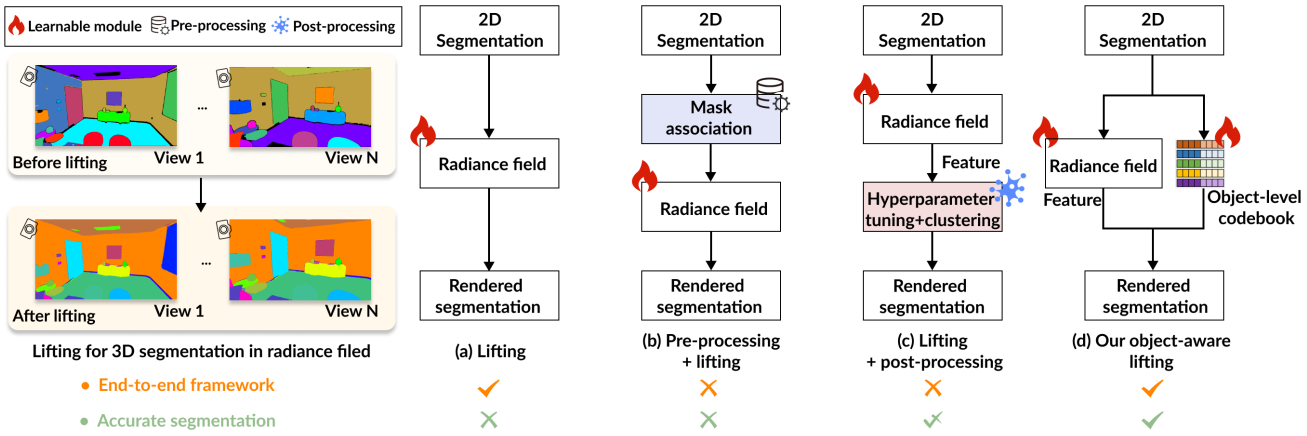

Figure 1. Comparing the pipeline of our method against previous lifting solutions.

ject in the 3D scene. This codebook is further associated with the rendered Gaussian-level features to predict segmentation results, enhancing object-level awareness during training. *However, effective codebook learning is non-trivial. Naive training solutions can lead to suboptimal performance.* Hence, we present effective learning strategies to optimize the object-level codebook. First, we introduce a novel association learning module, in which we design an area-aware ID mapping algorithm to generate pseudo-labels of association with enhanced multi-view consistency. Additionally, we present two complementary loss functions, *i.e.*, sparsity and concentration parts, to achieve more reliable object-level understanding. Second, we design a novel noisy label filtering module to enhance the robustness of our method by estimating an uncertainty map for the segmentation masks, leveraging the learned Gaussian-level features in a self-supervised manner. During inference, we obtain novel-view instance segmentation results without any pre- or post-processing, effectively avoiding error accumulation.

To evaluate the effectiveness of our Unified-Lift, we conduct experiments on the widely-used LERF-Masked [39] dataset and the indoor scene dataset, Replica [35]. Both quantitative and qualitative results demonstrate that our Unified-Lift outperforms all the existing lifting methods by a notable margin. Furthermore, we conduct additional experiments on the challenging Messy Rooms dataset [1], where each scene contains up to 500 objects, demonstrating the scalability of Unified-Lift in handling large numbers of objects.

Our main contributions are summarized as follows:

- We propose a new end-to-end *object-aware* lifting method (named Unified-Lift) for accurate 3D scene segmentation by jointly learning the Gaussian-level features and a global object-level codebook.
- We present a novel association learning module and a noisy label filtering module to facilitate effective learning of the object-level codebook.
- We set a new state-of-the-art performance on multiple datasets and demonstrate strong scalability in handling large numbers of objects without the need of pre- or post-processing.

2. Related Works

Radiance field: from implicit to explicit. Radiance field emerges as a promising representation for reconstructing 3D scenes with various properties, *e.g.*, geometries, colors, and semantics, from only 2D inputs such as RGB images and segmentation masks. Neural Radiance Field (NeRF) [25] models the radiance field using a neural network composed of layers of multilayer perceptrons. Since then, various works attempt to improve the efficiency of NeRF, *e.g.*, by explicitly formulating the field using 3D structures such as voxels [2, 22] and hash grids [27]. Later on, 3D Gaussian Splatting (3D-GS) [5, 11, 12, 21, 38, 41, 43] is introduced to model the radiance field as a set of explicit Gaussian points. This approach allows for a splatting-style rendering [16], which is highly efficient and demonstrates great potential of real-time rendering. Given the advantages, we employ 3D-GS as the backbone representation in our framework for creating consistent 3D segmentations.

Segmentation: from 2D to 3D. Segmentation is a long-standing task in computer vision research. Recent progress witnesses advancements in 2D, thanks to the availability of large-scale datasets. Notably, various foundation models, such as SAM [15] and its subsequent works [18, 37], show great performance in numerous 2D segmentation tasks and demonstrate robust zero-shot segmentation capabilities.

Beyond segmenting pixels in image level, 3D segmentation aims to partition 3D structures, such as point clouds and voxels [10, 26, 34, 45], or to perform segmentation and 3D reconstruction simultaneously from input 2D images [7, 28, 32]. However, due to tedious work needed in collecting annotated 3D data, the scale of 3D datasets (*e.g.*,

1,503 scenes in ScanNet [8]) is usually at least one order of magnitude smaller than that of 2D datasets (*e.g.*, 11M diverse images and 1.1B high-quality segmentation masks in SA-1B [15]). Hence, the trained models are applicable mostly to limited 3D object categories within the available dataset. To effectively construct 3D segmentation, we propose lifting the segmentation results from 2D foundation models by explicitly incorporating an object-level understanding of the 3D scene.

Lifting 2D segmentation to 3D scene understanding in radiance field. Various works [1, 30, 44] propose leveraging radiance fields to lift independently-inferred 2D information into the 3D space for 3D scene segmentation and understanding. Some works focus on semantic segmentation, aiming to infer semantic information in the 3D scene, such as object properties and categories, where 2D segmentation predictions are obtained via differentiable rendering. To accomplish this, most existing works tend to optimize a 3D radiance field, which is supervised by semantic or feature maps derived from 2D foundation models. For example, Semantic-NeRF [44] optimizes an additional semantic field from 2D semantic maps for novel-view semantic rendering. Besides, some studies [13, 19, 30, 42] distill CLIP [31] or DINO [29] features into a feature radiance field to facilitate open-vocabulary semantic segmentation.

Unlike semantic segmentation, instance segmentation predicted by 2D foundation models, such as SAM [15] and MaskFormer [3], lack consistency across multiple views. An early work, Panoptic Lifting [33], formulates the radiance field as a distribution of instance IDs and employs the Hungarian algorithm for each 2D segmentation to obtain pseudo labels as the supervision signal. To improve the performance, later works [9, 23, 39] attempt to pre-process the 2D instance segmentations (*e.g.*, using video tracker [4] or heuristic Gaussian matching [23]) to simplify the task and obtain view-consistent labels for supervision. Recent state-of-the-art methods [1, 6, 9, 14, 40, 46] construct 3D consistent feature fields and supervise them using contrastive loss within each 2D segmentation. This avoids the need to establish correspondences between different views. However, since radiance fields contain only features, inferring the final segmentation requires an additional clustering step, such as HDBSCAN [24], which can be rather sensitive to the choice of the hyperparameters. In this work, we propose a new end-to-end *object-aware lifting* pipeline for accurate 3D scene segmentation, avoiding the need of pre- or post-processing. By formulating an object-level codebook representation and designing dedicated modules for effective codebook learning, we obtain an object-level understanding of the scene to greatly enhance the segmentation quality.

3. Method

Given a set of posed images with 2D instance segmentation masks $\{\mathcal{K}\}$, our goal is to lift 2D segmentations to 3D and produce an accurate and consistent 3D segmentation of the scene, represented by the 3D Gaussian Splatting (3D-GS) model. In this work, we obtain the initial 2D masks using a zero-shot 2D segmentation model, specifically the Segment Anything Model (SAM). Fig. 2 illustrates the overview of our Unified-Lift, which consists of three major components. (i) We augment each Gaussian point in the 3D-GS representation with an additional Gaussian-level feature and employ contrastive loss to optimize the rendered Gaussian-level features (Fig. 2 top; detailed in Sec. 3.1). (ii) We impose an object-level understanding on the 3D scene to enhance segmentation quality by formulating an object-level codebook and associating the codebook with the Gaussian-level features through an object-Gaussians association for segmentation predictions (Fig. 2 bottom-left; detailed in Sec. 3.2). (iii) We introduce two novel modules for effective codebook learning based on the object-Gaussians association: the association learning module and the noisy label filtering module (Fig. 2 bottom-right: detailed in Sec. 3.3).

3.1. Learning Gaussian-level features

3D-GS backbone. The 3D Gaussian Splatting (3D-GS) model [12] encapsulates a 3D scene using explicit 3D Gaussians and utilizes differentiable rasterization for efficient rendering. Mathematically, 3D-GS aims to learn a set of N 3D Gaussian points $G = \{g_i\}_{i=1}^{N}$, where $g_i = \{\mathbf{p}_i, \mathbf{s}_i, \mathbf{q}_i, o_i, \mathbf{c}_i\}$ represents the trainable parameters for the i-th Gaussian point. The 3D Gaussian function $G_i(x)$ is defined by the center point $\mathbf{p}_i$, the scaling factor $\mathbf{s}_i$, and the quaternion $\mathbf{q}_i$. Moreover, o_i is the opacity value and $\mathbf{c}_i$ is the color values modeled by spherical harmonics coefficients. Following an efficient tile-based rasterization introduced in [12], the 3D Gaussian function G_i is first transformed to the 2D Gaussian function G_i' on the image plane. Then, a rasterizer is designed to sort the 2D Gaussians and employ the α-blending to compute the color $\mathbf{C}_u$ for the query pixel u: $\mathbf{C}_u = \sum_{i\in\mathcal{N}} \mathbf{c}_i \alpha_i \prod_{t=1}^{i-1}(1-\alpha_t), \alpha_i = o_i G_i'(u)$, where $\mathcal{N}$ is the number of sorted 2D Gaussians associated with pixel u. Subsequently, all parameters in $\{g_i\}_{i=1}^{N}$ are optimized using the photometric loss between the rendered colors and the observed image colors.

Contrastive learning for Gaussian-level features. To encode the instance segmentation information of the 3D scene, each 3D Gaussian point g_i is augmented with a Gaussian-level learnable feature $\mathbf{f}_i \in \mathbb{R}^d$, where d is the feature dimension. Similar to the color information, we can apply differentiable rasterization to efficiently render the feature $\mathbf{F}_u$ for pixel u: $\mathbf{F}_u = \sum_{i\in\mathcal{N}} \mathbf{f}_i \alpha_i \prod_{t=1}^{i-1}(1-\alpha_t), \alpha_i = o_i G_i'(u)$. Following existing state-of-the-art methods [1, 40], we employ the contrastive learning technique to op-

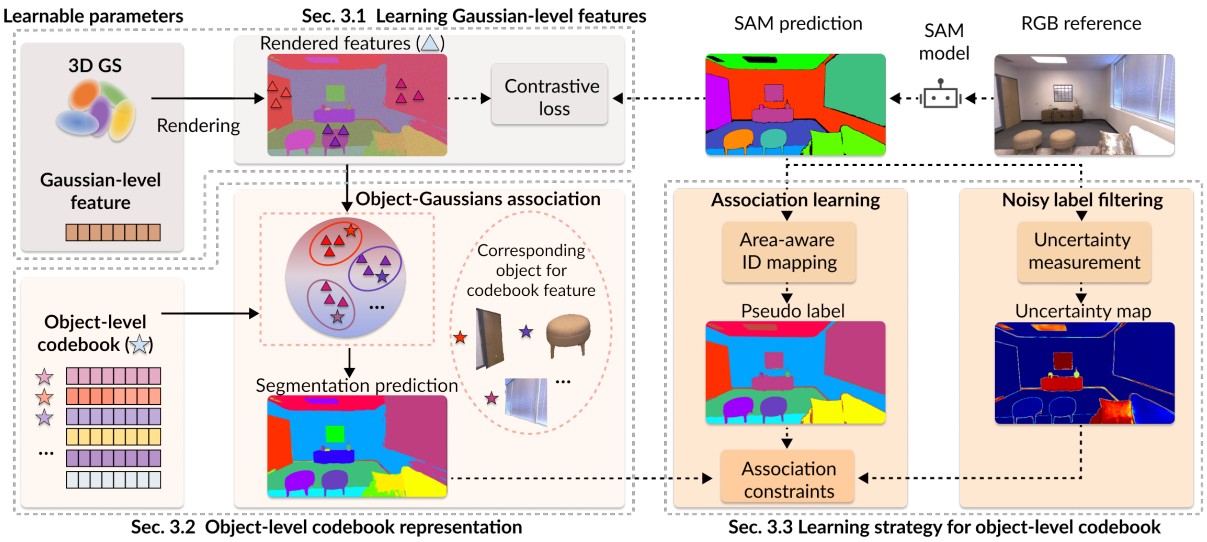

Figure 2. Overview of our Unified-Lift, which is built based on the 3D Gaussian Splatting (3D-GS) representation (top-left). In our pipeline, we first augment each Gaussian point in 3D-GS with a Gaussian-level feature and utilize the contrastive loss to optimize the rendered features (see top; detailed in Sec. 3.1). To impose an object-level understanding on the 3D scene, we introduce an additional object-level codebook and establish associations between the object-level features and the Gaussian-level features (see bottom-left; detailed in Sec. 3.2). Further, we propose two novel modules, the association learning module and the noisy label filtering module, to robustly and accurately learn the codebook (see bottom-right; detailed in Sec. 3.3).

timize the Gaussian-level features $\mathbf{f}_i$ from individual views. Specifically, we apply the following InfoNCE loss [20] to supervise the rendered features:

$$\mathcal{L}_{\text{contra}} = -\frac{1}{|\Omega|}\sum_{\Omega_j \in \Omega}\sum_{u \in \Omega_j} \log \frac{\exp\left(\text{sim}\left(\mathbf{F}_u, \overline{\mathbf{F}}_j\right)\right)}{\sum_{\Omega_l \in \Omega}\exp\left(\text{sim}\left(\mathbf{F}_u, \overline{\mathbf{F}}_l\right)\right)}, \tag{1}$$

where similarity kernel function sim uses the dot product operation here and Ω is the set of pixel samples. In specific, Ω_j denotes the pixel samples with the same instance ID j according to the 2D segmentation $\mathcal{K}$, $\overline{\mathbf{F}}_j$ and $\overline{\mathbf{F}}_l$ represent the mean features (centroids) for Ω_j and Ω_l, respectively.

3.2. Object-level codebook representation

While Gaussian-level features implicitly encode instance information within the scene, they lack explicit object-level understanding and require an additional clustering post-process to extract this information for segmentation prediction [1, 40]. Consequently, these instance predictions not only suffer from tedious hyperparameter tuning but also encounter issues such as under- or over-segmentation due to the accumulated errors (see, *e.g.*, Fig. 3). Hence, we aim to obtain an explicit object-level understanding of the 3D scene by jointly learning it with the Gaussian-level features, getting rid of the constraints of post-processing.

Object-level codebook. As shown in Fig. 2 bottom-right, based on the Gaussian-level features, we introduce a learnable and global object-level codebook representation to impose an object-level understanding of the 3D scene. Practically, we represent the object-level codebook as a compact

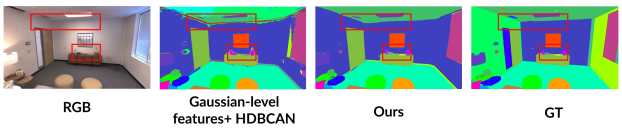

Figure 3. Visual comparisons. Segmentation results produced by our method and the Gaussian-level feature-based method [40] with post-processing [24]. Their result tends to overlook small objects and produces artifacts. In contrast, our method generates more accurate segmentations.

matrix $\mathbf{F}_{obj} := [\mathbf{F}^1_{obj}, \mathbf{F}^2_{obj}, \cdots, \mathbf{F}^L_{obj}]^T$, where $\mathbf{F}_{obj} \in \mathbb{R}^{L\times d}$, L is the maximum object number, and d denotes the same feature dimension used in the Gaussian-level features. Notably, each row in the matrix $\mathbf{F}_{obj}$ corresponds to an underlying object in the 3D scene.

We further establish the object-Gaussian association formulation to connect the object-level codebook with the Gaussian-level features. Given a pose, we render the feature map $\mathbf{F}$ from the optimized Gaussian-level features, with $\mathbf{F}_u \in \mathbb{R}^d$ denoting the feature for pixel u. Particularly, we propose the following association equation to calculate the probability distribution $\mathbf{P}_u \in \mathbb{R}^L$ for pixel u:

$$\mathbf{P}_u = [\frac{\exp\left(\text{sim}\left(\mathbf{F}_u, \mathbf{F}^1_{obj}\right)\right)}{\sum_{o=1}^{L}\exp\left(\text{sim}\left(\mathbf{F}_u, \mathbf{F}^o_{obj}\right)\right)}, \frac{\exp\left(\text{sim}\left(\mathbf{F}_u, \mathbf{F}^2_{obj}\right)\right)}{\sum_{o=1}^{L}\exp\left(\text{sim}\left(\mathbf{F}_u, \mathbf{F}^o_{obj}\right)\right)} , \cdots, \frac{\exp\left(\text{sim}\left(\mathbf{F}_u, \mathbf{F}^L_{obj}\right)\right)}{\sum_{o=1}^{L}\exp\left(\text{sim}\left(\mathbf{F}_u, \mathbf{F}^o_{obj}\right)\right)}], \tag{2}$$

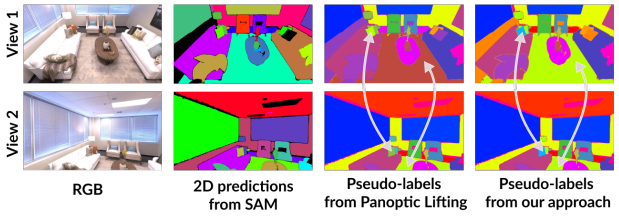

Figure 4. The comparison between the generated pseudo label results by Panoptic Lifting [33] and our method. With the designed area-aware ID mapping, we can obtain more view-consistent segmentation as the pseudo labels to facilitate the codebook learning.

where we use the same similarity kernel function sim as in Eq. 1, maintaining consistency with the learning of Gaussian-level features.

Baseline strategy for learning the object-level codebook. To automatically learn the object-level codebook during training, a straightforward solution is to directly optimize the object-Gaussians association predictions. To obtain the pseudo-labels for this optimization, we can match the 2D segmentation results with the current object-Gaussians association results via the linear assignment algorithm [17]. In practice, we first need to recover the mapping Π from the original instance IDs in the 2D segmentation to the global IDs $\{0, 1, 2, \cdots, L-1\}$ in the 3D scene. Following [33], the expected mapping $\Pi^\star$ is defined by:

$$\Pi^\star := \underset{\Pi}{\operatorname{argmax}} \sum_{\Omega_j \in \Omega} \sum_{u \in \Omega_j} \frac{\mathbf{P}_u\left(\Pi(j)\right)}{|\Omega_j|}, \tag{3}$$

where $\mathbf{P}_u\left(\Pi(j)\right)$ is the $\Pi(j)$-th value in the probability prediction $\mathbf{P}_u$. Then, we apply the cross-entropy loss as a sparsity term to regress the probability distribution based on calculated pseudo-labels:

$$\mathcal{L}_{\text{class}} := -\frac{1}{|\Omega|} \sum_{u \in \Omega} \log \mathbf{P}_u\left(\Pi^\star\left(\mathcal{K}_u\right)\right), \tag{4}$$

where the $\mathcal{K}_u$ is the instance ID for pixel u, given the 2D instance segmentation masks $\mathcal{K}$.

Inference with the object-level codebook. Benefiting from the learned explicit object-level codebook representation, our method achieves an end-to-end segmentation inference without the need for a complicated post-processing. In general, to render a segmentation in novel views, we first (i) render the Gaussian-level features; then (ii) calculate the probability using the object-Gaussians association equation; and (iii) determine the segmentation ID by selecting the index of the codebook that exhibits the highest similarity. Furthermore, the same association equation can be directly applied to determine the instance ID for each 3D Gaussian.

3.3. Learning strategy for object-level codebook

Although our baseline strategy for learning the codebook is technically feasible, it faces limitations in terms of performance and robustness. To address these challenges and improve codebook learning, we introduce two novel modules: the association learning module and the noisy label filtering module.

3.3.1. Association learning module

Our association learning module aims to improve the multi-view consistency of pseudo-labels and provide more robust association constraints. To achieve this, we introduce an area-aware ID mapping method and a concentration part to ensure more comprehensive association constraints.

Area-aware ID mapping. We observe that the ID mapping described in Eq. 2 is sensitive to the small segments in specific views, thereby further causing the multi-view inconsistency issue, as shown in Fig. 4, To mitigate this issue and improve the multi-view consistency of the generated pseudo-labels, we propose an area-aware ID mapping function, formulated as:

$$\Pi^\star := \underset{\Pi}{\operatorname{argmax}} \sum_{\Omega_j \in \Omega} \sum_{u \in \Omega_j} \mathbf{P}_u\left(\Pi(j)\right). \tag{5}$$

Compared to the previous formulation in Eq. 3, the key distinction lies in the removal of the normalization term. This design prioritizes the influence of large segments in the mapping process, resulting in more consistent mapping across views, as qualitatively shown in Fig. 4. More analysis is provided in Sec. 4.4 and the supplementary material.

Concentration constraint. We assume that the object-level features assigned in the codebook should align with the clustered Gaussian-level features. Moreover, the clustered Gaussian-level features, optimized using a contrastive loss with dot product similarity, tend to exhibit similar directions. Building on this insight, we propose an additional concentration constraint to minimize the directional differences between the codebook and all corresponding normalized Gaussian-level features:

$$\mathcal{L}_{\text{concen}} := \frac{1}{|\Omega|} \sum_{u \in \Omega} \|\mathbf{F}_{obj}^{\Pi^\star(\mathcal{K}_u)} - \mathbf{F}_u / \|\mathbf{F}_u\|\|_1. \tag{6}$$

Thus, we formulate the total association constraint loss as a linear combination of the sparsity component in Eq. 4 and the concentration component in Eq. 6, providing a comprehensive association constraint for the object-level codebook.

3.3.2. Noisy label filtering module

To enhance the robustness against noise in the 2D instance segmentation masks, we propose a filtering module that removes less accurate 2D predictions by leveraging multi-view consistently rendered Gaussian-level features. Specifically, we calculate the uncertainty value $\mathbf{W}_u$ for pixel u as

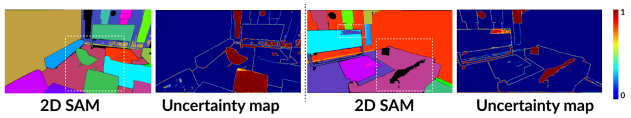

Figure 5. Visual comparison of the generated uncertainty maps and 2D instance segmentation masks from different views from the "Office3" scene in the Replica dataset [35].

$$\mathbf{W}_u = 1 - \frac{\exp\left(\text{sim}\left(\mathbf{F}_u, \overline{\mathbf{F}}_{(\mathcal{K}_u)}\right)\right)}{\sum_{\Omega_l \in \Omega} \exp\left(\text{sim}\left(\mathbf{F}_u, \overline{\mathbf{F}}_l\right)\right)}, \tag{7}$$

where $\overline{\mathbf{F}}_{(\mathcal{K}_u)}$ is the mean feature (centroid) for $\Omega_{(\mathcal{K}_u)}$. In practice, we model the uncertainty by assessing whether the features corresponding to the current 2D instance segmentation are sufficiently discriminative. Accordingly, we can effectively filter out labels with high uncertainty values (*i.e.*, noisy labels) and integrate this filtering into our association constraints. The overall loss for our proposed learning strategy of the object-level codebook is

$$\begin{aligned}\mathcal{L} = -\frac{1}{|\Omega|} \sum_{u \in \Omega} \mathbf{1}_{(\mathbf{W}_u \leq \tau)} \big(\underbrace{w_{\text{class}} \log \mathbf{P}_u\left(\Pi^\star\left(\mathcal{K}_u\right)\right)}_{\text{Sparsity part in Eq. 4}} + \\ \underbrace{w_{\text{concen}} \|\mathbf{F}_{obj}^{\Pi^\star(\mathcal{K}_u)} - \mathbf{F}_u / \|\mathbf{F}_u\|\|_1}_{\text{Concentration part in Eq. 6}} \big),\end{aligned} \tag{8}$$

where w_{class}, w_{concen} are weight hyper-parameters, and $\tau = 0.8$ is a pre-defined threshold for filtering noisy labels. As verified in Fig. 5, regions with high values in the calculated uncertainty map largely align with areas of noisy segmentation. More analysis can be found in Sec. 4.4.

4. Experiments

4.1. Experiments setting

Implementation details. Our implementation is based on the official codebase of 3D-GS [12]. We utilize the same photometric loss term in [12] to optimize the associated 3D Gaussian parameters. For the Gaussian-level features, we set the feature dimension to 16, following the baseline works such as OmniSeg3D-GS [40] and Gaussian Grouping [39]. To optimize the Gaussian-level features, we apply the same contrastive loss used in [40]. For the object-level codebook, we set the maximum object number L to 256 and use the proposed loss defined in Eq. 8 to optimize the object-level codebook from a random initialization. Empirically, we set $w_{\text{class}} = 1 \times 10^{-3}$ and $w_{\text{concen}} = 1 \times 10^{-1}$ by default. All parameters are jointly optimized, with the number of training iterations set to 30,000 for all datasets. More details are provided in the Supp.

Datasets. We conduct experiments on the widely-used LERF-Mask dataset [39] and the Replica dataset [35] to conduct both quantitative and qualitative comparisons. The LERF-Mask dataset includes three scenes, "figures", "ramen", and "teatime", each with six to ten object segmentation annotations. For the Replica dataset, we prepare our customized data and re-evaluate all comparative methods using this dataset since the data used in Gaussian Grouping [39] is not publicly available. Following the processing in [36], we select eight scenes for experiments. Besides, we use the official Segment Anything Model (SAM) [15] to make predictions and obtain the initial 2D segmentation masks, empirically choosing the largest granularity that provides the object-level segmentation context.

Method	Venue	Type	mIoU(%)	mBIoU (%)
LERF [13]	ICCV'23	CLIP feature	37.2	29.3
LangSplat [30]	CVPR'24	CLIP feature	57.6	53.6
Gaussian Grouping [39]	ECCV'24	Pre-processing	72.8	67.6
Gaga [23]	Arxiv'24	Pre-processing	74.7	72.2
OmniSeg3D-GS [40](†)	CVPR'24	Post-processing	74.7	71.8
Panoptic-Lifting-GS [33](*)	CVPR'23	End-to-end	70.7	65.8
Ours	-	End-to-end	80.9	77.1

Table 1. Results on LERF-Mask dataset. We report the mIoU and mBIoU$^{\text{scene}}$ metrics following Gaussian Grouping [39]. * indicates self-implementation, and † indicates that the results are reported under the best-found hyper-parameter (*i.e.*, minimal cluster size in HDBSCAN [24].

Method	Type	mIoU(%)	F-score (%)
Gaussian Grouping [39]	Pre-processing	23.6	30.4
OmniSeg3D-GS [40](†)	Post-processing	39.1	35.9
Panoptic-Lifting-GS [33](*)	End-to-end	25.3	32.9
Our	End-to-end	41.6	43.9

Table 2. Results on Replica dataset. We report the Maksed-mIoU, mIoU, and F-score metrics. * indicates self-implementation, and † indicates that the results are reported under the best-found hyper-parameter (*i.e.*, minimal cluster size for HDBSCAN [24]).

Metrics. For the LERF-Mask dataset, we adopt the evaluation protocol from [39] following the existing works [23, 39], using the mean Intersection over Union (mIoU) and the boundary IoU (mBIoU) metrics. For the Replica dataset, we first use the linear assignment algorithm to calculate the best matching of IoU between the segmentation predictions and ground-truth data; we then report both the mIoU metric and F-score, using an IoU threshold of 0.5 as the criterion.

Comparisons. We compare our proposed method with three types of lifting approaches based on 3D-GS: (i) lifting methods with a preprocessing, such as Gaussian Grouping [39] and Gaga [23]; (ii) the lifting method with a post-processing, *i.e.*, OmniSeg3D-GS [40]; and (iii) a direct lifting baseline (*i.e.*, "Panoptic-Lifting-GS" denoted in Tab. 1, Tab. 2, and Tab. 3) that is derived from Panoptic-Lifting [33]. To ensure fair comparisons, we evaluate the OmniSeg3D-GS baseline using the HDBSCAN [24] algorithm to automatically generate segmentation results. Further, we report metrics under the best-found hyper-parameters, following the common practice used in [1]. Moreover, we benchmark our method against the recent open-vocabulary 3D segmentation techniques, including LERF [13] and Lansplat [30].

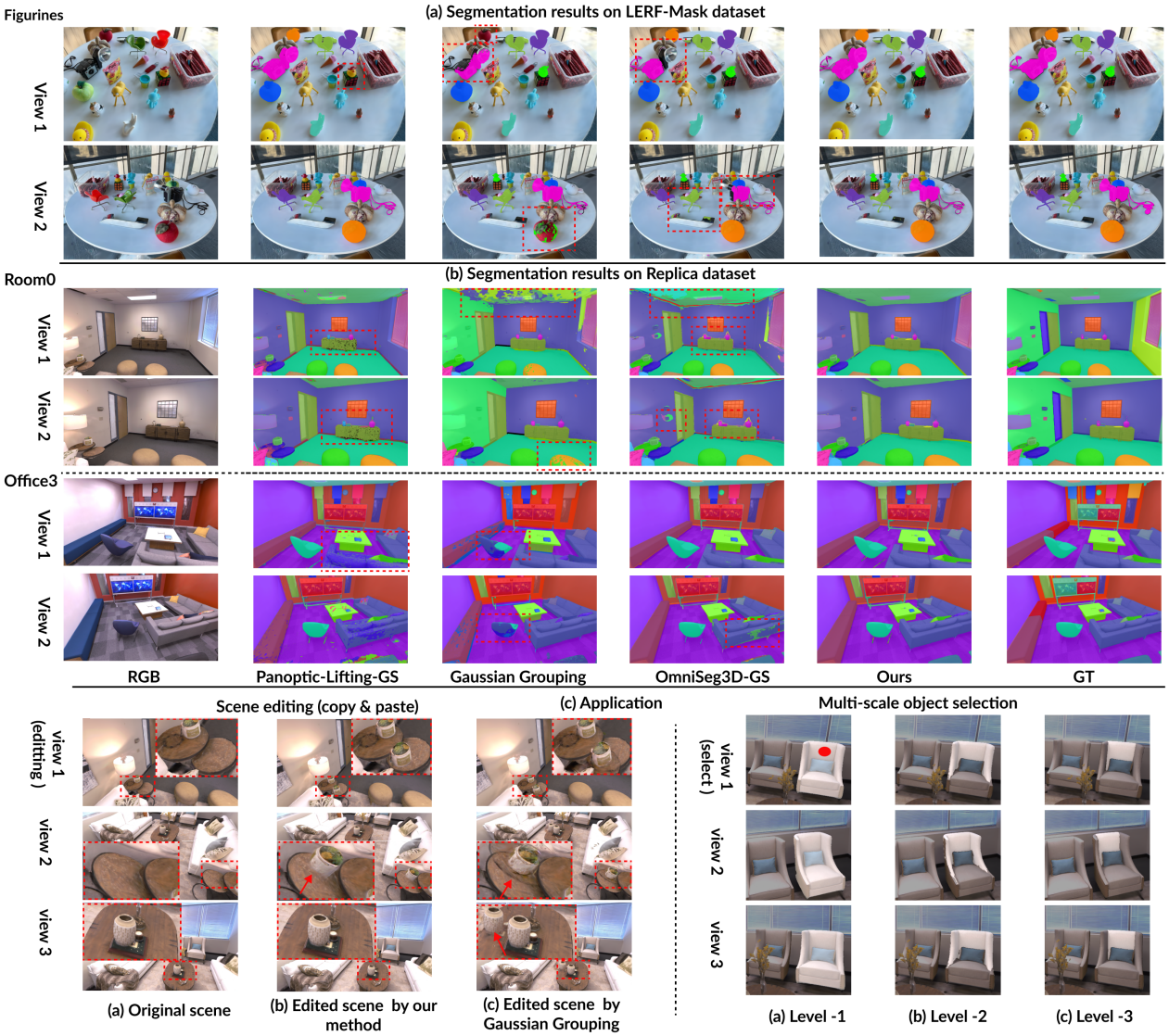

Figure 6. Qualitative comparison of our Unified-Lift with previous methods. We provide visual comparisons on the LERF-Masked dataset [39] in (a); and on the Replica dataset [35] in (b). Moreover, we present the application results in (c). As shown in the left part of (c), we select the potted plants in view 1 and apply the copy & paste operations to the associated Gaussian points. The consistent editing results in view 2 and view further demonstrate the advantages of our method. In contrast, using segmentations derived from Gaussian Grouping [39] leads to severe artifacts and can even adversely affect unrelated object such as the vase observed in view 3. In addition, we illustrate the multi-scale object selection application in the right part of (c). By clicking on the red point in view 1, we consistently select the sofa instance at three different granularities across multiple views.

Backbone	Type	Method/ Number	Old Room Environment (%)				Large Corridor Environment(%)				**Mean(%)**	**Training (h)**
			25	50	100	500	25	50	100	500		
NeRF	End-to-end	Panoptic Lifting [33]	73.2	69.9	64.3	51.0	65.5	71.0	61.8	49.0	63.2	≥ 20
	Post-processing	Contrastive Lift [1]	78.9	75.8	69.1	55.0	76.5	75.5	68.7	52.5	69.0	≥ 20
GS	Post-processing	OmniSeg3D-GS [40](†)	80.1	72.4	61.4	46.8	74.9	79.6	63.9	48.5	66.0	≈ 1
	End-to-end	Panoptic-Lifting-GS [33](*)	67.5	65.1	59.4	46.1	62.2	65.3	57.5	45.5	58.6	≈ 1
	End-to-end	Ours	79.1	72.2	65.9	53.9	77.0	78.9	70.7	54.1	69.0	≈ 1

Table 3. Results on the Messy Rooms dataset [1]. Following [1], PQ^{scene} metric is reported on both the "old room" and "large corridor" environments with an increasing number of objects in the scene $(25, 50, 100, 500)$. * indicates self-implementation, and † indicates that the results are reported under the best-found hyper-parameter (*i.e.*, minimal cluster size for HDBSCAN [24]). Note that, we test the training time for all methods using a single NVIDIA 3090 RTX GPU.

Method	mIoU(%)	F-score (%)
Previous end-to-end baseline [33]	25.3	32.9
Our baseline solution (with codebook)	29.5	39.2
+ concentration constraint	36.3	41.3
+ area-aware ID mapping	39.2	41.0
+ noisy label filtering (full method)	41.6	43.9

Table 4. Ablation study on the Replica [35] dataset.

4.2. Main experiments

LERF-Mask dataset. To evaluate performance on real-world data, we conduct the experiments using the LERF-Mask dataset [39]. Quantitative comparisons provided in Tab. 1 demonstrate that our Unified-Lift outperforms all existing lifting methods, as well as open-vocabulary approaches like LERF [13] and Lansplat [30]. Moreover, visual comparisons between our Unified-Lift and other methods are presented in Fig. 6 (a), demonstrating the effectiveness of our approach in achieving consistent and accurate 3D segmentation. Following the process in the baseline work [39], we set the segmentation result to empty if the calculated IoU between predictions and ground truth falls below a predefined threshold.

Replica dataset. To further validate the effectiveness of our Unified-Lift, we conduct experiments on the Replica dataset [35], which comprises eight distinct scenes. Quantitative comparisons with state-of-the-art methods, presented in Tab. 2, demonstrate that our Unified-Lift achieves the best performances across all metrics. Visual results, illustrated in Fig. 6 (b), further verify that our method not only produces more accurate segmentations for small objects (*e.g.*, vase and button) but also generates significantly fewer artifacts compared to the existing methods. Notably, even when using the optimal hyper-parameters in HDBSCAN [24] for OmniSeg3D-GS [40], its post-processing clustering algorithm struggles to balance accuracy for small objects and smooth segmentation for larger objects.

4.3. Scalability on varying object numbers

To demonstrate the scalability of our Unified-Lift across varying object quantities, we conduct additional experiments on the widely-used Messy Rooms dataset [1], which covers scenes containing up to 500 distinct objects. For fair comparisons, we follow the same evaluation protocol used in the previous work [1] to calculate the metric that assesses the consistency of instance IDs across multiple views [33], denoting as PQ^{scene} in Tab. 3. Specifically, we choose the segment with largest area in the generated instance segmentation across different views as the background, to generate the binary semantic segmentations for PQ^{scene} metric calculations. This approach avoids the need to optimize an additional semantic feature in our method, as well as in all 3D-GS-based baselines. We compare our method with the 3D-GS-based baselines (*i.e.*, OmniSeg3D-GS and Panoptic-Lifting-GS) and the NeRF-based baselines (*i.e.*, Panoptic Lifting [33] and Contrastive Lift [1]) for a comprehensive evaluation. As shown in Tab. 3, the quantitative results demonstrate that our method achieves improved performance compared to 3D-GS-based baselines, particularly in scenes with a large number of objects. Moreover, our method achieves results comparable to the current state-of-the-art NeRF-based method [1], while requiring significantly less training time.

4.4. Ablation study

We conduct a detailed ablation study to validate the effectiveness of each component in our proposed method. Quantitative results presented in Tab. 4 show that our new end-to-end lifting method, combined with a baseline codebook learning solution, achieves improved performance compared to the previous end-to-end baseline (*i.e.*, Panoptic-Lifting-GS [33]). Moreover, each proposed learning strategy further enhances our method's performance.

4.5. Applications

Our method effectively offers an object-level understanding of the 3D scene, which can further facilitate downstream applications. For example, it enables the direct selection of objects in the 3D domain for fundamental copy-and-paste operations. Benefiting from our accurate segmentation results, the edited outputs appear more natural and exhibit fewer artifacts, as illustrated in Fig. 6 (c) left. Furthermore, our method can be easily extended to provide multi-granularity understanding, by simply employing segmentation at various granularities (*e.g.*, three-level granularity for SAM). This capability enables end-to-end multi-scale object selections, as showcased in Fig. 6 (c) right.

5. Conclusion

We propose a new end-to-end object-aware lifting approach, Unified-Lift, based on 3D-GS for constructing accurate and efficient 3D scene segmentations. Specifically, we introduce a novel object-level codebook to incorporate an explicit object-level understanding of the 3D scene by learning a representation for each object. Method-wise, we first augment each Gaussian point with a Gaussian-level point feature and adopt the contrastive loss to optimize these features. Then, we formulate the object-level codebook representation and associate it with the Gaussian-level features for object-aware segmentation prediction. To ensure effective and robust learning for the object-level codebook, we further propose the association learning module and the noisy label filtering module. Extensive experimental results manifest the effectiveness of our method over the state of the arts, without the need of pre- or post-processing. Further analysis on the Messy Rooms dataset also shows its scalability in handling large numbers of objects.

Acknowledgement

This work is supported by the InnoHK Clusters of the Hong Kong SAR Government via the Hong Kong Centre for Logistics Robotics; and the Research Grants Council of the Hong Kong Special Administrative Region, China, under Project CUHK 14200824.

References

[1] Yash Bhalgat, Iro Laina, João F Henriques, Andrew Zisserman, and Andrea Vedaldi. Contrastive Lift: 3D object instance segmentation by slow-fast contrastive fusion. *arXiv preprint arXiv:2306.04633*, 2023. 1, 2, 3, 4, 6, 7, 8

[2] Anpei Chen, Zexiang Xu, Andreas Geiger, Jingyi Yu, and Hao Su. Tensorf: Tensorial radiance fields. In *European Conference on Computer Vision*, pages 333–350. Springer, 2022. 2

[3] Bowen Cheng, Ishan Misra, Alexander G Schwing, Alexander Kirillov, and Rohit Girdhar. Masked-attention mask transformer for universal image segmentation. In *Proceedings of the IEEE/CVF conference on computer vision and pattern recognition*, pages 1290–1299, 2022. 1, 3

[4] Ho Kei Cheng, Seoung Wug Oh, Brian Price, Alexander Schwing, and Joon-Young Lee. Tracking anything with decoupled video segmentation. In *Proceedings of the IEEE/CVF International Conference on Computer Vision*, pages 1316–1326, 2023. 3

[5] Kai Cheng, Xiaoxiao Long, Kaizhi Yang, Yao Yao, Wei Yin, Yuexin Ma, Wenping Wang, and Xuejin Chen. Gaussianpro: 3d gaussian splatting with progressive propagation. In *Forty-first International Conference on Machine Learning*, 2024. 2

[6] Seokhun Choi, Hyeonseop Song, Jaechul Kim, Taehyeong Kim, and Hoseok Do. Click-gaussian: Interactive segmentation to any 3d gaussians. *arXiv preprint arXiv:2407.11793*, 2024. 3

[7] Manuel Dahnert, Ji Hou, Matthias Nießner, and Angela Dai. Panoptic 3D scene reconstruction from a single rgb image. *Advances in Neural Information Processing Systems*, 34: 8282–8293, 2021. 2

[8] Angela Dai, Angel X Chang, Manolis Savva, Maciej Halber, Thomas Funkhouser, and Matthias Nießner. Scannet: Richly-annotated 3D reconstructions of indoor scenes. In *Proceedings of the IEEE conference on computer vision and pattern recognition*, pages 5828–5839, 2017. 3

[9] Bin Dou, Tianyu Zhang, Yongjia Ma, Zhaohui Wang, and Zejian Yuan. Cosseggaussians: Compact and swift scene segmenting 3d gaussians with dual feature fusion. *CoRR*, 2024. 3

[10] Stefano Gasperini, Mohammad-Ali Nikouei Mahani, Alvaro Marcos-Ramiro, Nassir Navab, and Federico Tombari. Panoster: End-to-end panoptic segmentation of LiDAR point clouds. *IEEE Robotics and Automation Letters*, 6(2):3216–3223, 2021. 2

[11] Binbin Huang, Zehao Yu, Anpei Chen, Andreas Geiger, and Shenghua Gao. 2d gaussian splatting for geometrically accurate radiance fields. In *ACM SIGGRAPH 2024 Conference Papers*, pages 1–11, 2024. 2

[12] Bernhard Kerbl, Georgios Kopanas, Thomas Leimkühler, and George Drettakis. 3D gaussian splatting for real-time radiance field rendering. *ACM Transactions on Graphics*, 42 (4), 2023. 1, 2, 3, 6

[13] Justin Kerr, Chung Min Kim, Ken Goldberg, Angjoo Kanazawa, and Matthew Tancik. LERF: Language embedded radiance fields. In *Proceedings of the IEEE/CVF International Conference on Computer Vision*, pages 19729–19739, 2023. 3, 6, 8

[14] Chung Min Kim, Mingxuan Wu, Justin Kerr, Ken Goldberg, Matthew Tancik, and Angjoo Kanazawa. Garfield: Group anything with radiance fields. In *Proceedings of the IEEE/CVF Conference on Computer Vision and Pattern Recognition*, pages 21530–21539, 2024. 3

[15] Alexander Kirillov, Eric Mintun, Nikhila Ravi, Hanzi Mao, Chloe Rolland, Laura Gustafson, Tete Xiao, Spencer Whitehead, Alexander C Berg, Wan-Yen Lo, et al. Segment anything. *arXiv preprint arXiv:2304.02643*, 2023. 1, 2, 3, 6

[16] Georgios Kopanas, Julien Philip, Thomas Leimkühler, and George Drettakis. Point-based neural rendering with per-view optimization. In *Computer Graphics Forum*, pages 29–43. Wiley Online Library, 2021. 2

[17] Harold W Kuhn. The hungarian method for the assignment problem. *Naval research logistics quarterly*, 2(1-2):83–97, 1955. 5

[18] Feng Li, Hao Zhang, Peize Sun, Xueyan Zou, Shilong Liu, Jianwei Yang, Chunyuan Li, Lei Zhang, and Jianfeng Gao. Semantic-sam: Segment and recognize anything at any granularity. *arXiv preprint arXiv:2307.04767*, 2023. 2

[19] Hao Li, Roy Qin, Zhengyu Zou, Diqi He, Bohan Li, Bingquan Dai, Dingewn Zhang, and Junwei Han. Langsurf: Language-embedded surface gaussians for 3d scene understanding. *arXiv preprint arXiv:2412.17635*, 2024. 3

[20] Junnan Li, Pan Zhou, Caiming Xiong, and Steven CH Hoi. Prototypical contrastive learning of unsupervised representations. *arXiv preprint arXiv:2005.04966*, 2020. 4

[21] Zhihao Liang, Qi Zhang, Wenbo Hu, Ying Feng, Lei Zhu, and Kui Jia. Analytic-splatting: Anti-aliased 3d gaussian splatting via analytic integration. *arXiv preprint arXiv:2403.11056*, 2024. 2

[22] Lingjie Liu, Jiatao Gu, Kyaw Zaw Lin, Tat-Seng Chua, and Christian Theobalt. Neural sparse voxel fields. *Advances in Neural Information Processing Systems*, 33:15651–15663, 2020. 2

[23] Weijie Lyu, Xueting Li, Abhijit Kundu, Yi-Hsuan Tsai, and Ming-Hsuan Yang. Gaga: Group any gaussians via 3d-aware memory bank. *arXiv preprint arXiv:2404.07977*, 2024. 1, 3, 6

[24] Leland McInnes, John Healy, and Steve Astels. hdbscan: Hierarchical density based clustering. *J. Open Source Softw.*, 2(11):205, 2017. 3, 4, 6, 7, 8

[25] Ben Mildenhall, Pratul P Srinivasan, Matthew Tancik, Jonathan T Barron, Ravi Ramamoorthi, and Ren Ng. NeRF: Representing scenes as neural radiance fields for view synthesis. *Communications of the ACM*, 65(1):99–106, 2021. 2

[26] Andres Milioto, Jens Behley, Chris McCool, and Cyrill Stachniss. LiDAR panoptic segmentation for autonomous

driving. In *2020 IEEE/RSJ International Conference on Intelligent Robots and Systems (IROS)*, pages 8505–8512. IEEE, 2020. 2

[27] Thomas Müller, Alex Evans, Christoph Schied, and Alexander Keller. Instant neural graphics primitives with a multiresolution hash encoding. *ACM transactions on graphics (TOG)*, 41(4):1–15, 2022. 2

[28] Gaku Narita, Takashi Seno, Tomoya Ishikawa, and Yohsuke Kaji. Panopticfusion: Online volumetric semantic mapping at the level of stuff and things. In *2019 IEEE/RSJ International Conference on Intelligent Robots and Systems (IROS)*, pages 4205–4212. IEEE, 2019. 2

[29] Maxime Oquab, Timothée Darcet, Théo Moutakanni, Huy Vo, Marc Szafraniec, Vasil Khalidov, Pierre Fernandez, Daniel Haziza, Francisco Massa, Alaaeldin El-Nouby, et al. Dinov2: Learning robust visual features without supervision. *arXiv preprint arXiv:2304.07193*, 2023. 3

[30] Minghan Qin, Wanhua Li, Jiawei Zhou, Haoqian Wang, and Hanspeter Pfister. Langsplat: 3d language gaussian splatting. In *Proceedings of the IEEE/CVF Conference on Computer Vision and Pattern Recognition*, pages 20051–20060, 2024. 3, 6, 8

[31] Alec Radford, Jong Wook Kim, Chris Hallacy, Aditya Ramesh, Gabriel Goh, Sandhini Agarwal, Girish Sastry, Amanda Askell, Pamela Mishkin, Jack Clark, et al. Learning transferable visual models from natural language supervision. In *International conference on machine learning*, pages 8748–8763. PMLR, 2021. 3

[32] Antoni Rosinol, Arjun Gupta, Marcus Abate, Jingnan Shi, and Luca Carlone. 3D dynamic scene graphs: Actionable spatial perception with places, objects, and humans. *arXiv preprint arXiv:2002.06289*, 2020. 2

[33] Yawar Siddiqui, Lorenzo Porzi, Samuel Rota Bulò, Norman Müller, Matthias Nießner, Angela Dai, and Peter Kontschieder. Panoptic lifting for 3D scene understanding with neural fields. In *Proceedings of the IEEE/CVF Conference on Computer Vision and Pattern Recognition*, pages 9043–9052, 2023. 1, 3, 5, 6, 7, 8

[34] Kshitij Sirohi, Rohit Mohan, Daniel Büscher, Wolfram Burgard, and Abhinav Valada. Efficientlps: Efficient LiDAR panoptic segmentation. *IEEE Transactions on Robotics*, 38 (3):1894–1914, 2021. 2

[35] Julian Straub, Thomas Whelan, Lingni Ma, Yufan Chen, Erik Wijmans, Simon Green, Jakob J Engel, Raul Mur-Artal, Carl Ren, Shobhit Verma, et al. The replica dataset: A digital replica of indoor spaces. *arXiv preprint arXiv:1906.05797*, 2019. 2, 6, 7, 8

[36] Matias Turkulainen, Xuqian Ren, Iaroslav Melekhov, Otto Seiskari, Esa Rahtu, and Juho Kannala. Dn-splatter: Depth and normal priors for gaussian splatting and meshing. *arXiv preprint arXiv:2403.17822*, 2024. 6

[37] Yunyang Xiong, Bala Varadarajan, Lemeng Wu, Xiaoyu Xiang, Fanyi Xiao, Chenchen Zhu, Xiaoliang Dai, Dilin Wang, Fei Sun, Forrest Iandola, et al. Efficientsam: Leveraged masked image pretraining for efficient segment anything. In *Proceedings of the IEEE/CVF Conference on Computer Vision and Pattern Recognition*, pages 16111–16121, 2024. 2

[38] Tian-Xing Xu, Wenbo Hu, Yu-Kun Lai, Ying Shan, and Song-Hai Zhang. Texture-gs: Disentangling the geometry and texture for 3d gaussian splatting editing. *arXiv preprint arXiv:2403.10050*, 2024. 2

[39] Mingqiao Ye, Martin Danelljan, Fisher Yu, and Lei Ke. Gaussian grouping: Segment and edit anything in 3D scenes. *arXiv preprint arXiv:2312.00732*, 2023. 1, 2, 3, 6, 7, 8

[40] Haiyang Ying, Yixuan Yin, Jinzhi Zhang, Fan Wang, Tao Yu, Ruqi Huang, and Lu Fang. Omniseg3d: Omniversal 3d segmentation via hierarchical contrastive learning. In *Proceedings of the IEEE/CVF Conference on Computer Vision and Pattern Recognition*, pages 20612–20622, 2024. 1, 3, 4, 6, 7, 8

[41] Zehao Yu, Anpei Chen, Binbin Huang, Torsten Sattler, and Andreas Geiger. Mip-splatting: Alias-free 3d gaussian splatting. In *Proceedings of the IEEE/CVF Conference on Computer Vision and Pattern Recognition*, pages 19447–19456, 2024. 2

[42] Hao Zhang, Fang Li, and Narendra Ahuja. Open-nerf: Towards open vocabulary nerf decomposition. In *Proceedings of the IEEE/CVF Winter Conference on Applications of Computer Vision*, pages 3456–3465, 2024. 3

[43] Zheng Zhang, Wenbo Hu, Yixing Lao, Tong He, and Hengshuang Zhao. Pixel-gs: Density control with pixel-aware gradient for 3d gaussian splatting. *arXiv preprint arXiv:2403.15530*, 2024. 2

[44] Shuaifeng Zhi, Tristan Laidlow, Stefan Leutenegger, and Andrew J Davison. In-place scene labelling and understanding with implicit scene representation. In *Proceedings of the IEEE/CVF International Conference on Computer Vision*, pages 15838–15847, 2021. 1, 3

[45] Zixiang Zhou, Yang Zhang, and Hassan Foroosh. Panoptic-polarnet: Proposal-free LiDAR point cloud panoptic segmentation. In *Proceedings of the IEEE/CVF Conference on Computer Vision and Pattern Recognition*, pages 13194–13203, 2021. 2

[46] Runsong Zhu, Shi Qiu, Qianyi Wu, Ka-Hei Hui, Pheng-Ann Heng, and Chi-Wing Fu. Pcf-lift: Panoptic lifting by probabilistic contrastive fusion. In *European Conference on Computer Vision*, pages 92–108. Springer, 2024. 3